

A modified fifth-order WENO scheme for hyperbolic conservation laws

Samala Rathan*, G Naga Raju †

Department of Mathematics, Visvesvaraya National Institute of Technology, Nagpur, India

Abstract

This paper deals with a new fifth-order weighted essentially non-oscillatory (WENO) scheme improving the WENO-NS and WENO-P methods which are introduced in Ha et al. J. Comput. Phys. (2013) and Kim et al., J. Sci. Comput. (2016) respectively. These two schemes provide the fifth-order accuracy at the critical points where the first derivatives vanish but the second derivatives are non-zero. In this paper, we have presented a scheme by defining a new global-smoothness indicator which shows an improved behavior over the solution to the WENO-NS and WENO-P schemes and the proposed scheme attains optimal approximation order, even at the critical points where the first and second derivatives vanish but the third derivatives are non-zero.

Keywords: Hyperbolic conservation laws, WENO scheme, smoothness indicators, non-linear weights, discontinuity.

MSC: 65M20, 65N06, 41A10.

1 Introduction

The hyperbolic conservation laws may develop discontinuities in its solution even if the initial conditions are smooth. Therefore classical numerical methods which depend on Taylor's expansion fails, so the spurious oscillations occur in the solution. To resolve this, the Total Variation Diminishing (TVD) schemes are constructed by Harten in [10, 11] based on the principle that, the total variation to the approximation of numerical solution must be non-increasing in time. But the TVD schemes are at most first order accurate near smooth extrema [20].

In order to overcome this difficulty, Harten et al. [12, 13, 14] succeeded by relaxing the TVD condition and allowing the spurious oscillations to occur in the numerical scheme, but the $O(1)$ Gibbs-like phenomena are essentially prevented. This is the first successful higher order spatial discretization method for the hyperbolic conservation laws that achieves the essentially non-oscillatory (ENO) property and known as ENO schemes. In [12], finite-volume ENO method was studied and shown that, to have a uniform high-order accuracy right up to the location of any discontinuity. Later, the finite-difference ENO scheme was developed by Shu and Osher in [24, 25].

The ENO method works based on the idea of choosing the interpolation points over a stencil which avoids the initiation of oscillations in the numerical solution. To do this, a smoothness

*Email: rathan.maths@gmail.com

†Email: gnagaraju@mth.vnit.ac.in

indicator of the solution is determined over each stencil and by using this, the smoothest candidate stencil is chosen from a set of candidate stencils. As the result, the ENO scheme avoids spurious oscillations near discontinuities and obtains information from smooth regions only.

The weighted ENO (WENO) scheme is introduced by Liu et al. [19], in the finite-volume framework up to third-order of accuracy and later, Jiang and Shu [17], introduced this WENO scheme in finite-difference framework which we refer here as WENO-JS scheme by constructing the new smoothness indicators that measure the sum of the normalized squares of the scaled L_2 norms of all derivatives of local interpolating polynomials. Very high order schemes are constructed in [2] based on the WENO-JS scheme which satisfies monotonicity preserving property.

The main idea behind the WENO scheme is that it uses a convex combination of all the ENO candidate sub-stencils in a non-linear manner and assigns a weight to each sub-stencil between 0 and 1 based on its local smoothness indicator. The basic strategy of assigning the weights is that, by the combining of the lower order polynomials with optimal weights, which yields an upwind scheme of maximum possible order in smooth regions of the solution and assigns smaller weights to those lower order polynomials whose stencils contain discontinuities so that the essentially non-oscillatory property is achieved. The detailed description of the methodology about ENO and WENO schemes and their implementation can be found in [22, 23].

It is first pointed out by Henrick et al. in [15], that the desired convergence rate of the fifth-order WENO-JS was not achieved for many problems where the first and third derivatives of the flux do not simultaneously vanish and the behavior of the scheme is sensitive to ϵ , a parameter is introduced in order to avoid division by zero in the evaluation of non-linear weights. They suggested an improved version of the WENO-JS scheme which is termed as mapped WENO and abbreviated by WENO-M. By using a mapping function on the nonlinear weights, WENO-M satisfies the sufficient condition where WENO-JS fails and obtains an optimal order of convergence near simple smooth extrema. Consequently, higher order WENO schemes were developed based on mapping function in [7].

In a different approach to the construction of the nonlinear weights, Borges et al. [3], introduced the fifth-order WENO-Z scheme. In their study, the authors measured the smoothness of the large stencil which comprises all sub-stencils and incorporated this in devising the smoothness indicators and nonlinear weights. The resulting WENO-Z scheme is less dissipative than WENO-JS and WENO-M. The convergence order of the WENO-Z scheme is four at the first-order critical points and degrade to two when higher order critical points are encountered. Further, a closed-form formula was derived in [4] for the WENO-Z scheme to the all odd orders, higher than fifth-order accuracy.

The smoothness indicators based on Lagrange interpolation polynomials are derived in [5] which gives the desired order of convergence if the first and second derivatives vanish but the third derivatives are non-zero by constructing the higher-order global smoothness indicator in L_2 -sense. The resulting scheme shows less dissipative nature than other schemes and subsequently high order schemes were presented in [6]. Modified smoothness indicators of WENO-JS scheme is presented in [16] based on the linear combination of second order derivatives over the global stencil by using the idea of WENO-Z scheme. Acker et al. in [1], have observed that the improving the weights information where the solution is non-smooth is more important than the improving the accuracy at critical points. To do this, they introduced an extra term to the WENO-Z weights so that the scheme behaves with the same stability and sharpness as the WENO-Z scheme at discontinuities and shocks with a higher numerical resolution. The WENO methodology is still in development to improve its rate of convergence in smooth regions and decrease the dissipation near the discontinuities even it is successful in a wide number of applications.

Recently Ha et al. [9] introduced the local as well as global smoothness indicators based on L_1 -norm approach and termed this scheme as WENO-NS. The WENO-NS scheme provides an improved behavior compared to other fifth-order WENO schemes for the problems which contain discontinuities. It is well known that the smoothness indicators constructed based on L_1 -norm approach may lead to provide loss of regularity of the solution. To overcome this difficulty, the authors constructed local smoothness indicators by developing an approximation method to derivatives with higher accuracy and introduce a parameter ξ in calculating the local smoothness indicators to the tradeoff between the accuracy around the smooth and discontinuous regions. The global smoothness indicator is constructed as an average of the smoothness of a global stencil data and a middle stencil information through a mapping function which satisfies desirable sufficient condition so that the scheme achieves required order of accuracy.

The main difficulty in WENO-NS scheme is to find global smoothness indicator and because of the symmetry nature of the two local smoothness indicators in the WENO-NS scheme out of three, the given three sub-stencils may provide the unbalanced contribution to the evaluation of flux at the interface. Kim et al. [18], made a balanced tradeoff among all the sub-stencils by introducing a parameter δ in the formulation of local smoothness indicators and constructed a global smoothness indicator which does not include an extra information like as in WENO-NS scheme i.e., middle stencil data. This modification yields better performance than the WENO-NS scheme and termed as WENO-P scheme.

A simple analysis verifies that the resulting WENO-NS and WENO-P schemes have the fifth-order accuracy if the first-order critical point vanish but the second derivatives are non-zero. The main aim of this study is to further improve the WENO-NS and WENO-P schemes to achieve desired order of accuracy even if the first and second derivatives vanish but the third derivative is non-zero.

In this article, we analyzed the fifth-order WENO scheme with the smoothness indicators developed in [17, 15, 3, 9, 18] and derived a new global smoothness indicator which is a linear combination of second order derivatives leads to give a fourth-order of accuracy so, the resulting global smoothness indicator provides a much smoother information to the evaluation point in evaluating the non-linear weights. It is verified that the proposed WENO scheme has the fifth-order accuracy even at critical points where first and second derivatives vanish but the third derivative is non-zero through the Taylor expansion. We call this scheme as modified WENO-P (MWENO-P) which takes almost the same computational cost as that of WENO-NS or WENO-P and is simple to implement as the WENO-JS or WENO-Z schemes. The numerical experiments are shown that the proposed scheme MWENO-P performs better than WENO-JS, WENO-Z, WENO-NS and WENO-P for the problems which contain discontinuities.

The organization of the paper is as follows. Preliminaries to understand about WENO reconstructions to the one-dimensional scalar conservation laws are presented in section 2 and in section 3 details about the construction of a new global measurement which estimates smoothness of a local solution in the construction of a fifth-order WENO scheme. Some numerical results are provided in Section 4 to demonstrate advantages of the proposed WENO scheme. Finally, concluding remarks are given in Section 5.

2 WENO schemes

Consider the general form of conservation law

$$u_t + f(u)_x = 0, -\infty < x < \infty, t > 0, \quad (1)$$

with initial condition

$$u(x, 0) = u_0(x).$$

Here the function $u = (u_1, u_2, \dots, u_m)^T$ is a m -dimensional vector of conserved variables, flux $f(u)$ is a vector-valued function of m components, x and t denote space and time variables respectively. The system is called hyperbolic if all the eigen values $\lambda_1, \lambda_2, \dots, \lambda_m$ of the Jacobian matrix $A = \frac{\partial f}{\partial u}$, of the flux function are real and set of right eigen vectors are complete.

Let $\{I_j\}$ be a partition of a spatial domain with the j^{th} cell $I_j = [x_{j-\frac{1}{2}}, x_{j+\frac{1}{2}}]$, where $x_{j\pm\frac{1}{2}}$ are called cell interfaces. The centre of each cell I_j is denoted by $x_j = \frac{1}{2}(x_{j+\frac{1}{2}} + x_{j-\frac{1}{2}})$ and the value of the function at the node x_j is denoted by $f_j = f(x_j)$. We assume that the set $\{x_{j+\frac{1}{2}}\}_j$ is uniformly spatial gridded throughout the domain and the cell size of I_j is denoted by $\Delta x = x_{j+\frac{1}{2}} - x_{j-\frac{1}{2}}$. The approximation of one-dimensional hyperbolic conservation laws (1) leads to system of ordinary differential equations by applying the method of lines, where the finite difference approximation is replaced to the spatial derivative and yields a semi discrete scheme

$$\frac{du_j}{dt} = -\frac{1}{\Delta x}(\hat{f}_{j+\frac{1}{2}} - \hat{f}_{j-\frac{1}{2}}). \quad (2)$$

Here u_j is the approximation to the point value $u(x_j, t)$ and $\hat{f}_{j\pm\frac{1}{2}}$ are called numerical fluxes which are Lipschitz continuous in each of its arguments and is consistent with the physical flux $\hat{f}(u, \dots, u) = f(u)$. The conservation property is obtained by defining a function $h(x)$ implicitly through the following equation (see Lemma 2.1 of [25])

$$f(u(x, .)) = \frac{1}{\Delta x} \int_{x_{j-\frac{1}{2}}}^{x_{j+\frac{1}{2}}} h(\xi) d\xi. \quad (3)$$

Differentiating (3) with respect to x yields

$$f(u(x, .))_x = \frac{1}{\Delta x}(h(x_{j+\frac{1}{2}}) - h(x_{j-\frac{1}{2}})), \quad (4)$$

where $h(x_{j\pm\frac{1}{2}})$ is a approximation to the numerical flux $\hat{f}_{j\pm\frac{1}{2}}$ with a high order of accuracy, that is,

$$\hat{f}_{j\pm\frac{1}{2}} = h(x_{j\pm\frac{1}{2}}) + O(\Delta x^r). \quad (5)$$

To ensure the numerical stability and to avoid entropy violating solutions, the flux $f(u)$ is splitted into two parts f^+ and f^- , thus

$$f(u) = f^+(u) + f^-(u), \quad (6)$$

where $\frac{df^+(u)}{du} \geq 0$ and $\frac{df^-(u)}{du} \leq 0$.

The numerical fluxes $\hat{f}_{j+\frac{1}{2}}^+$ and $\hat{f}_{j+\frac{1}{2}}^-$ evaluates at $x_{j+\frac{1}{2}}$ obtained from (3) which are positive and negative parts of $f(u)$ respectively and with this we have $\hat{f}_{j+\frac{1}{2}} = \hat{f}_{j+\frac{1}{2}}^+ + \hat{f}_{j+\frac{1}{2}}^-$. We will only describe how $\hat{f}_{j+\frac{1}{2}}^+$ is approximated because the negative part of the split flux, is symmetric to the positive part with respect to $x_{j+\frac{1}{2}}$. For brevity, we drop the '+' sign in the superscript from here onwards.

2.1 Fifth order WENO schemes

The WENO schemes are designed for the approximation to the spatial derivative to solve the hyperbolic conservation laws, which are used to reconstruct the unknown values of a given flux function f from its known values in an essentially non-oscillatory manner. To construct $\hat{f}_{j+\frac{1}{2}}$, the classical fifth-order WENO scheme uses five point stencil $S^5 = \{x_{j-2}, x_{j-1}, x_j, x_{j+1}, x_{j+2}\}$ which is subdivided into three candidate sub-stencils $S_0(j), S_1(j)$ and $S_2(j)$. To each cell I_j , the corresponding stencil is denoted by

$$S_k(j) = \{x_{j+k-2}, x_{j+k-1}, x_{j+k}\}, \quad k = 0, 1, 2$$

and let

$$\hat{f}_{j+\frac{1}{2}}^k = \sum_{q=0}^2 c_{k,q} f_{j+k+q-2},$$

be the second-degree polynomial constructed on the stencil $S_k(j)$ to approximate the value $h(x_{j+\frac{1}{2}})$ where the coefficients $c_{k,q} (q = 0, 1, 2)$ are the Lagrange's interpolation coefficients depending on the shifting parameter k . The flux values on each stencil can be written in the form of

$$\begin{aligned} \hat{f}_{j+\frac{1}{2}}^0 &= \frac{1}{6}(2f_{j-2} - 7f_{j-1} + 11f_j), \\ \hat{f}_{j+\frac{1}{2}}^1 &= \frac{1}{6}(-f_{j-1} + 5f_j + 2f_{j+1}), \\ \hat{f}_{j+\frac{1}{2}}^2 &= \frac{1}{6}(2f_j + 5f_{j+1} - f_{j+2}). \end{aligned} \tag{7}$$

The flux $\hat{f}_{j-\frac{1}{2}}^k$ is obtained through shifting the index by -1 . The Taylor expansion of (7) reveals

$$\begin{aligned} \hat{f}_{j\pm\frac{1}{2}}^0 &= h_{j\pm\frac{1}{2}} - \frac{1}{4}f'''(0)\Delta x^3 + O(\Delta x^4), \\ \hat{f}_{j\pm\frac{1}{2}}^1 &= h_{j\pm\frac{1}{2}} + \frac{1}{12}f'''(0)\Delta x^3 + O(\Delta x^4), \\ \hat{f}_{j\pm\frac{1}{2}}^2 &= h_{j\pm\frac{1}{2}} - \frac{1}{12}f'''(0)\Delta x^3 + O(\Delta x^4). \end{aligned}$$

The convex combination of these flux functions define the approximation to the value of $h(x_{j+\frac{1}{2}})$ which is

$$\hat{f}_{j+\frac{1}{2}} = \sum_{k=0}^2 \omega_k \hat{f}_{j+\frac{1}{2}}^k, \tag{8}$$

where ω_k are the non-linear weights. If the function $h(x)$ is smooth in all the sub-stencils $S_k(j)$, $k = 0, 1, 2$, we calculate the constants d_k such that its linear combination with $\hat{f}_{j+\frac{1}{2}}^k$ gives the fifth order convergence to $h(x_{j+\frac{1}{2}})$, that is,

$$h_{j+\frac{1}{2}} = \sum_{k=0}^2 d_k \hat{f}_{j+\frac{1}{2}}^k + O(\Delta x^5).$$

The coefficients d_k are known as the ideal weights because they generate the upstream central fifth-order scheme for the five-point stencil. The values of ideal weights are given by

$$d_0 = 1/10, \quad d_1 = 6/10, \quad d_2 = 3/10. \tag{9}$$

The non-linear weights ω_k are defined in (8) as

$$\omega_k = \frac{\alpha_k}{\sum_{q=0}^2 \alpha_q}, \quad (10)$$

and

$$\alpha_k = \frac{d_k}{(\epsilon + \beta_k)^2}, \quad (11)$$

where $0 < \epsilon \ll 1$ is introduced to prevent the denominator becoming zero and β_k is a smoothness indicator of the flux \hat{f}^k which measures the smoothness of a solution over a particular stencil. The necessary and sufficient conditions to achieve the fifth-order convergence for the WENO scheme are

$$\sum_{k=0}^2 (\omega_k^\pm - d_k) = O(\Delta x^6), \quad (12)$$

$$\sum_{k=0}^2 A_k (\omega_k^+ - \omega_k^-) = O(\Delta x^3), \quad (13)$$

$$\omega_k^\pm - d_k = O(\Delta x^2). \quad (14)$$

Since (12) holds always due to the normalization, a sufficient condition for the fifth-order convergence to the scheme is derived in [3] as

$$\omega_k^\pm - d_k = O(\Delta x^3), \quad (15)$$

where the superscripts $'+'$ and $'-'$ on ω_k correspond to their use in either $f_{j+\frac{1}{2}}^k$ and $f_{j-\frac{1}{2}}^k$ respectively.

2.1.1 The WENO-JS scheme

The suggested smoothness indicators β_k of Jiang and Shu in [17] are given by

$$\beta_k = \sum_{q=1}^2 \Delta x^{2q-1} \int_{x-\frac{\Delta x}{2}}^{x+\frac{\Delta x}{2}} \left(\frac{d^q \hat{f}^k}{dx^q} \right)^2 dx. \quad (16)$$

The explicit form of the these smoothness indicators are as follows:

$$\begin{aligned} \beta_0 &= \frac{13}{12}(f_{j-2} - 2f_{j-1} + f_j)^2 + \frac{1}{4}(f_{j-2} - 4f_{j-1} + 3f_j)^2, \\ \beta_1 &= \frac{13}{12}(f_{j-1} - 2f_j + f_{j+1})^2 + \frac{1}{4}(f_{j+1} - f_{j-1})^2, \\ \beta_2 &= \frac{13}{12}(f_j - 2f_{j+1} + f_{j+2})^2 + \frac{1}{4}(3f_j - 4f_{j+1} + f_{j+2})^2. \end{aligned} \quad (17)$$

By the Taylor's expansion of these smoothness indicators, one obtain

$$\begin{aligned} \beta_0 &= f'^2 \Delta x^2 + \left(\frac{13}{12} f''^2 - \frac{2}{3} f' f''' \right) \Delta x^4 + \left(\frac{-13}{6} f'' f''' + \frac{1}{2} f' f^{(4)} \right) \Delta x^5 + O(\Delta x^6), \\ \beta_1 &= f'^2 \Delta x^2 + \left(\frac{13}{12} f''^2 + \frac{1}{3} f' f''' \right) \Delta x^4 + O(\Delta x^6), \\ \beta_2 &= f'^2 \Delta x^2 + \left(\frac{13}{12} f''^2 - \frac{2}{3} f' f''' \right) \Delta x^4 + \left(\frac{13}{6} f'' f''' - \frac{1}{2} f' f^{(4)} \right) \Delta x^5 + O(\Delta x^6). \end{aligned}$$

The smoothness indicators (17) are smoother than the smoothness indicators presented in [19], which are constructed based on the total variation measurement of a stencil in L_1 -norm. The Taylor expansion of these smoothness indicators β_k satisfies the sufficient condition

$$\beta_k = D(1 + O(\Delta x^2)),$$

where the constant D is independent of k but depends on the Δx , which implies that the WENO weights satisfy the condition

$$\omega_k - d_k = O(\Delta x^2).$$

Therefore, the final WENO reconstruction provides the fifth order convergence in the smooth regions. However at the critical points where the first derivative of f vanishes, the convergence property may not hold since $\beta_k = D(1 + O(\Delta x))$ yields $\omega_k - d_k = O(\Delta x)$. Further, the order of convergence is degraded to two if the first derivative and second derivatives vanish but the third derivative is non-zero .

2.1.2 WENO-M

When the fifth-order WENO-JS scheme is used, the condition (15) may not hold at certain smooth extrema or near critical points, yielding the third-order accuracy. To overcome this situation Henrick et al. [15] introduced a mapping function $g_k(\omega)$ as

$$g_k(\omega) = \frac{\omega(d_k + d_k^2 - 3d_k\omega + \omega^2)}{d_k^2 + \omega(1 - 2d_k)}, k = 0, 1, 2, \quad (18)$$

where d_k 's are the ideal weights and $\omega \in [0, 1]$. This function is a non-decreasing monotone function on $[0, 1]$ which satisfies the following properties

$$\begin{aligned} (i) & 0 \leq g_k(\omega) \leq 1, g_k(0) = 0 \text{ and } g_k(1) = 1. \\ (ii) & g_k(\omega) \approx 0 \text{ if } \omega \approx 0, g_k(\omega) \approx 1 \text{ if } \omega \approx 1. \\ (iii) & g_k(d_k) = d_k, g'_k(d_k) = g''_k(d_k) = 0. \\ (iv) & g_k(\omega) = d_k + O(\Delta x^6), \text{ if } \omega = d_k + O(\Delta x^2) \end{aligned} \quad (19)$$

and with this mapping function, non-linear weights are defined as

$$\omega_k^M = \frac{\alpha_k^M}{\sum_{l=0}^2 \alpha_l^M} \text{ and } \alpha_k^M = g_k(\omega_k^{JS}), k = 0, 1, 2, \quad (20)$$

where ω_k^{JS} are computed in (10) with the WENO-JS scheme by using the smoothness indicators defined in (16).

2.1.3 WENO-Z

Borges et al. [3] presented a scheme, known as WENO-Z, by introducing global smoothness indicator. The idea is to use whole five point stencil S^5 to define a new smoothness indicator of higher order than the classical smoothness indicator β_k , as

$$\tau_5 = |\beta_0 - \beta_2|. \quad (21)$$

By Taylor's expansion, the truncation error of τ_5 is

$$\tau_5 = \frac{13}{3} |f'' f'''| \Delta x^5 + O(\Delta x^6), \quad (22)$$

and the smoothness indicators are defined as

$$\beta_k^z = \frac{\beta_k + \epsilon}{\beta_k + \epsilon + \tau_5}, \quad k = 0, 1, 2, \quad (23)$$

and finally with this local smoothness indicators, the WENO weights are defined as

$$\omega_k^z = \frac{\alpha_k^z}{\sum_{q=0}^2 \alpha_q^z}, \quad \alpha_k^z = \frac{d_k}{\beta_k^z} = d_k \left(1 + \left[\frac{\tau_5}{\beta_k + \epsilon} \right]^p \right), \quad k = 0, 1, 2, \quad (24)$$

where ϵ is chosen as a very small value in order to force this parameter to play only its original role of not allowing vanishing denominator for each weight and with the value $p = 1$ in (24), the scheme achieves the fourth order accuracy and with $p = 2$, the scheme achieves the fifth-order accuracy.

2.1.4 The WENO-NS scheme

Ha et al., have introduced smoothness indicators based on L_1 - norm in [9] which measures the smoothness of a solution on each 3-point stencil $S_k(j)$, $k = 0, 1, 2$ by estimating the approximate magnitude of derivatives as

$$\beta_k = \xi |L_{1,k}f| + |L_{2,k}f|, \quad (25)$$

where the operators $L_{n,k}f$, $k = 0, 1, 2$ are the generalized undivided differences, defined by

$$|L_{1,k}f| = (1-k)f_{j-2+k} + (2k-3)f_{j-1+k} + (2-k)f_{j+k}, \quad (26)$$

$$|L_{2,k}f| = f_{j-2+k} - 2f_{j-1+k} + f_{j+k}. \quad (27)$$

The number ξ is a parameter which is to balance the tradeoff between the accuracy around the smooth regions and the discontinuous regions. The second term $L_{2,k}f$ is the same as the ones of the WENO-JS scheme, however, this scheme uses the absolute values while the later uses the squared ones. The advantage with these operators $L_{n,k}f$ is that the approximation of the derivative $\Delta x^n f^{(n)}$ at the point, $x_{j+\frac{1}{2}}$ with the high order of accuracy can be obtained, that is,

$$L_{n,k}f = \frac{d^n f}{dx^n}(x_{j+\frac{1}{2}}) + O(\Delta x^3). \quad (28)$$

By using Theorem 3.2 of [9], the Taylor's expansion of β'_k s are

$$\begin{aligned} \beta_0 &= \xi \left| \Delta x f_{j+\frac{1}{2}}^{(1)} - \frac{23}{24} \Delta x^3 f_{j+\frac{1}{2}}^{(3)} \right| + \left| \Delta x^2 f_{j+\frac{1}{2}}^{(2)} - \frac{3}{2} \Delta x^3 f_{j+\frac{1}{2}}^{(3)} \right| + O(\Delta x^4), \\ \beta_1 &= \xi \left| \Delta x f_{j+\frac{1}{2}}^{(1)} + \frac{1}{24} \Delta x^3 f_{j+\frac{1}{2}}^{(3)} \right| + \left| \Delta x^2 f_{j+\frac{1}{2}}^{(2)} - \frac{1}{2} \Delta x^3 f_{j+\frac{1}{2}}^{(3)} \right| + O(\Delta x^4), \\ \beta_2 &= \xi \left| \Delta x f_{j+\frac{1}{2}}^{(1)} + \frac{1}{24} \Delta x^3 f_{j+\frac{1}{2}}^{(3)} \right| + \left| \Delta x^2 f_{j+\frac{1}{2}}^{(2)} + \frac{1}{2} \Delta x^3 f_{j+\frac{1}{2}}^{(3)} \right| + O(\Delta x^4). \end{aligned} \quad (29)$$

The non-linear weights are defined as

$$\omega_k^{NS} = \frac{\alpha_k^{NS}}{\sum_{q=0}^2 \alpha_q^{NS}}, \quad \alpha_k^{NS} = d_k \left(1 + \frac{\zeta}{(\beta_k + \epsilon)^2} \right), \quad k = 0, 1, 2, \quad (30)$$

where

$$\zeta = \frac{1}{2}(|\beta_0 - \beta_2|^2 + g(L_{1,1}f)^2), \quad g(x) = \frac{x^3}{1 + x^3} \quad (31)$$

so that the sufficient condition $\omega_k^\pm - d_k = O(\Delta x^3)$ holds even first derivative vanish but the second derivative is non-zero.

2.1.5 The WENO-P scheme

The drawback of WENO-NS scheme is that all the three sub-stencils $S_0(j)$, $S_1(j)$ and $S_2(j)$ may provide unbalanced contribution to the evaluation point $x_{j+\frac{1}{2}}$ because, the stencils $S_1(j)$ and $S_2(j)$ are symmetric with respect to the point $x_{j+\frac{1}{2}}$ whereas $S_0(j)$ is not. Therefore the interpolation process may be over-influenced to the evaluation point from the left sub-stencils. For this, in [18] the authors improved the WENO-NS scheme by adjusting smoothness indicators to the three sub-stencils by

$$\tilde{\beta}_0 = \beta_0, \quad \tilde{\beta}_1 = (1 + \delta)\beta_1, \quad \tilde{\beta}_2 = (1 - \delta)\beta_2. \quad (32)$$

They also observed that the global smoothness measurement which uses an additional contribution term which measures the regularity of a solution over the stencil $S_1(j)$. Instead of using the measurement proposed in WENO-NS scheme and to save computational cost, they proposed WENO-P scheme with modification to the weights as

$$\omega_k^P = \frac{\alpha_k^P}{\sum_{q=0}^2 \alpha_q^P}, \quad \alpha_k^P = d_k \left(1 + \frac{\zeta}{(\tilde{\beta}_k + \epsilon)^2} \right), \quad k = 0, 1, 2, \quad (33)$$

where

$$\zeta = (\beta_0 - \beta_2)^2,$$

and these weights satisfy the sufficient condition to get fifth order accuracy when the first derivative vanishes but not the second derivative.

3 A new WENO scheme

To achieve the desired fifth-order accuracy when the first and second derivatives vanish but the third derivative is non-zero, a modified WENO-P scheme called MWENO-P is proposed here.

The Taylor's expansion of the operators $L_{n,k}f$ defined in (26, 27) by using Theorem 3.2 of [9] are

$$\begin{aligned}
L_{1,0}f &= \Delta x f_{j+\frac{1}{2}}^{(1)} - \frac{23}{24} \Delta x^3 f_{j+\frac{1}{2}}^{(3)} + \Delta x^4 f_{j+\frac{1}{2}}^{(4)} + O(\Delta x^5), \\
L_{1,1}f &= \Delta x f_{j+\frac{1}{2}}^{(1)} + \frac{1}{24} \Delta x^3 f_{j+\frac{1}{2}}^{(3)} + O(\Delta x^5), \\
L_{1,2}f &= \Delta x f_{j+\frac{1}{2}}^{(1)} + \frac{1}{24} \Delta x^3 f_{j+\frac{1}{2}}^{(3)} + O(\Delta x^5), \\
L_{2,0}f &= \Delta x^2 f_{j+\frac{1}{2}}^{(2)} - \frac{3}{2} \Delta x^3 f_{j+\frac{1}{2}}^{(3)} + \frac{29}{384} \Delta x^4 f_{j+\frac{1}{2}}^{(4)} + O(\Delta x^5), \\
L_{2,1}f &= \Delta x^2 f_{j+\frac{1}{2}}^{(2)} - \frac{1}{2} \Delta x^3 f_{j+\frac{1}{2}}^{(3)} + \frac{5}{24} \Delta x^4 f_{j+\frac{1}{2}}^{(4)} + O(\Delta x^5), \\
L_{2,2}f &= \Delta x^2 f_{j+\frac{1}{2}}^{(2)} + \frac{1}{2} \Delta x^3 f_{j+\frac{1}{2}}^{(3)} + \frac{5}{24} \Delta x^4 f_{j+\frac{1}{2}}^{(4)} + O(\Delta x^5).
\end{aligned} \tag{34}$$

The main idea is here to construct a high-order global smoothness indicator which is to satisfy the sufficient condition (15) if the first and second derivatives vanish but the third derivative is non-zero. Also the use of higher global smoothness indicator incurs the less dissipation near the discontinuities in the numerical scheme [5]. To construct such a global smooth measurement, we define a variable η as

$$\eta = |L_{2,0}f + L_{2,2}f - 2L_{2,1}f|^2.$$

which is a linear combination of undivided differences of second-order derivatives leads to give a fourth-order of accuracy, so this leads to give a much smooth measurement than the global smoothness indicators presented in [9, 18]. The Taylor's expansion of η yields

$$\begin{aligned}
\eta &= \left| -\frac{51}{384} \Delta x^4 f_{j+\frac{1}{2}}^{(4)} + O(\Delta x^5) \right|^2, \\
&= \Delta x^8 (A + O(\Delta x)^2),
\end{aligned}$$

and we define the new non-linear weights as

$$\omega_k^{MP} = \frac{\alpha_k^{MP}}{\sum_{q=0}^2 \alpha_q^{MP}}, \quad \alpha_k^{MP} = d_k \left(1 + \frac{\eta}{(\tilde{\beta}_k + \epsilon)^2} \right), \quad k = 0, 1, 2. \tag{35}$$

3.1 Convergence order at critical points

Here we discuss the convergence analysis of the proposed scheme MWENO-P at the critical points, that is how the new weights ω_k^{MP} are approaching the ideal weights d_k in the presence of critical points. First, consider that there is no critical point and assume that $\epsilon = 0$, then the local smoothness indicators $\tilde{\beta}_k$, as defined in (32) with weights as in (35) are of the form

$$\tilde{\beta}_k = |\Delta x f_{j+\frac{1}{2}}^{(1)}| + |\Delta x^2 f_{j+\frac{1}{2}}^{(2)}| + O(\Delta x^3) \tag{36}$$

and the global smoothness indicator is of the form

$$\eta = O(\Delta x^8) \tag{37}$$

By substituting equations (36) and (37) in (35), the sufficient condition (15) immediately holds so that the scheme has fifth convergence order.

If $f'_{j+\frac{1}{2}} = 0$ and $f''_{j+\frac{1}{2}} \neq 0$, the smoothness indicators are of the form

$$\tilde{\beta}_k = |f''_{j+\frac{1}{2}}| \Delta x^2 (1 + O(\Delta x))$$

then there is a constant D such that

$$\begin{aligned} 1 + \frac{\eta}{\tilde{\beta}_k^2} &= 1 + D\Delta x^4 + O(\Delta x^5) \\ &= (1 + D\Delta x^4) \left(1 + \frac{O(\Delta x^5)}{1 + D\Delta x^4} \right) \\ &= D_{\Delta x} (1 + O(\Delta x^5)) \end{aligned} \quad (38)$$

where $D_{\Delta x} = (1 + D\Delta x^4) > 0$. By substituting (38) in (35), then the sufficient condition holds hence the scheme has the fifth-order convergence at the first-order critical points.

Finally, if $f'_{j+\frac{1}{2}} = 0$, $f''_{j+\frac{1}{2}} = 0$ and $f'''_{j+\frac{1}{2}} \neq 0$, the smoothness indicators takes the form

$$\tilde{\beta}_k = |f'''_{j+\frac{1}{2}}| \Delta x^3 (1 + O(\Delta x)),$$

then there exist a constant \hat{D} such that

$$\begin{aligned} 1 + \frac{\eta}{\tilde{\beta}_k^2} &= 1 + \hat{D}\Delta x^2 + O(\Delta x^3) \\ &= (1 + \hat{D}\Delta x^2) \left(1 + \frac{O(\Delta x^3)}{1 + \hat{D}\Delta x^2} \right) \\ &= \hat{D}_{\Delta x} (1 + O(\Delta x^3)) \end{aligned} \quad (39)$$

where $\hat{D}_{\Delta x} = (1 + \hat{D}\Delta x^2) > 0$. By substituting equation (39) in (35), one can see that the sufficient condition holds and so the newly defined smoothness indicators attain the fifth-order convergence even in the case where first and second derivatives vanish but the third derivatives are non-zero.

4 Numerical Results

For time evaluation in (2) third-order TVD Runge-Kutta scheme (TVD RK3),

$$\begin{aligned} u^{(1)} &= u^n + \Delta t L(u^n), \\ u^{(2)} &= \frac{3}{4}u^n + \frac{1}{4}u^{(1)} + \frac{1}{4}\Delta t L(u^{(1)}), \\ u^{n+1} &= \frac{1}{3}u^n + \frac{2}{3}u^{(2)} + \frac{2}{3}\Delta t L(u^{(2)}). \end{aligned} \quad (40)$$

and fourth-order non-TVD Runge-Kutta schemes (RK-4),

$$\begin{aligned} u^{(1)} &= u^n + \frac{1}{2}\Delta t L(u^n), \\ u^{(2)} &= u^n + \frac{1}{2}\Delta t L(u^{(1)}), \\ u^{(3)} &= u^n + \Delta t L(u^{(2)}), \\ u^{n+1} &= \frac{1}{3}(-u^n + u^{(1)} + 2u^{(2)} + u^{(3)}) + \frac{1}{6}\Delta t L(u^{(3)}). \end{aligned} \quad (41)$$

where L is the spatial operator, are used in following numerical examples for evaluating the approximate solution using the proposed scheme MWENO-P.

The elaborate details of the schemes (40,41) can be found in [8]. The computed solution of MWENO-P is compared with WENO-JS, WENO-Z, WENO-NS and WENO-P schemes. All the numerical results are obtained on machine having an Intel(R) core (TM) i7 – 4700MQ processor with 8 GB of memory. In order to ensure fairness in the comparison, all the schemes shared the same subroutine calls and were compiled with the same compilation options. The only differences between the implementation of the WENO schemes were on the subroutines for computing the corresponding weights. In order to compare with the classical scheme, WENO-JS, we took $\epsilon = 10^{-6}$ and $\epsilon = 10^{-40}$ for WENO-Z, WENO-NS, WENO-P and MWENO-P schemes in all the following test cases. To prove the effectiveness of the scheme we considered various examples. For convergence analysis we first evaluated examples of scalar equation and later we have presented results for Euler equations.

4.1 Scalar test examples

The convergence analysis of the schemes is presented here by considering linear advection and Burger's equations with various initial profiles. Some of these initial profiles contain jump discontinuity and in some cases, the solution in time leads to contact discontinuity and shock. Here we've used the fifth-order flux version of WENO scheme based on Lax-Friedrich's flux splitting technique and time step is taken as $\Delta t \sim (\Delta x)^{\frac{5}{4}}$ so that the fourth order non-TVD Runge-Kutta method in time is effectively fifth-order. For all the examples in this subsection we've chosen $\xi = 0.1$ to evaluate the equation (25) and $\delta = 0.05$ to evaluate the equation (32).

4.1.1 Example 1:

Consider the transport equation

$$u_t + u_x = 0, \quad -1 \leq x \leq 1, \quad t \geq 0, \quad (42)$$

with the initial condition

$$u(x, 0) = \sin(\pi x), \quad (43)$$

and

$$u(x, 0) = \sin(\pi x - \frac{1}{\pi} \sin(\pi x)), \quad (44)$$

to test the numerical convergence of the proposed scheme. Below in Table 1 and Table 2, the L_1 and L_∞ errors are calculated up to time $t = 2$ for WENO-JS, WENO-NS and WENO-P schemes along with the proposed MWENO-P scheme for the initial condition (43). We observed that MWENO-P scheme converges slowly to the desired order of convergence for the approximate solution. The initial condition (44) is a special case to test the order of convergence since its first derivative vanishes but second derivative is non-zero. Here too, the numerical order of convergence for the MWENO-P scheme is more accurate when compared with WENO-JS, WENO-NS and WENO-P schemes which are shown in Table 3 and Table 4.

N	WENO JS	WENO-NS	WENO-P	MWENO-P
10	4.8506e-02(—)	4.4448e-02(—)	5.4913e-02(—)	9.2794e-03(—)
20	2.5414e-03(4.25)	2.1541e-03(4.36)	3.1845e-03(4.10)	3.0628e-04(4.92)
40	8.9204e-05(4.83)	3.0544e-05(6.14)	5.0576e-05(5.97)	1.0249e-05(4.90)
80	2.7766e-06(5.00)	3.1879e-07(6.58)	8.3516e-07(5.92)	3.1929e-07(5.00)
160	8.6040e-08(5.01)	9.9380e-09(5.00)	1.3716e-08(5.92)	9.9414e-09(5.00)
320	2.5528e-09(5.07)	3.1007e-10(5.00)	3.0641e-10(5.48)	3.1008e-10(5.00)

Table 1: L_∞ errors of linear advection Eq. (42) with initial condition (43)

N	WENO-JS	WENO-NS	WENO-P	MWENO-P
10	3.1593e-02(—)	3.1974e-02(—)	3.7323e-02(—)	5.2290e-03(—)
20	1.5177e-03(4.37)	8.6517e-04(5.27)	1.3817e-03(4.75)	2.1156e-04(4.62)
40	4.5188e-05(5.06)	9.8706e-06(6.45)	1.8070e-05(6.25)	6.6182e-06(4.99)
80	1.4000e-06(5.01)	2.1181e-07(5.54)	2.0924e-07(6.43)	2.0420e-07(5.01)
160	4.3621e-08(5.00)	6.3443e-09(5.06)	5.5174e-09(5.24)	6.3409e-09(5.00)
320	1.3600e-09(5.00)	1.9759e-10(5.00)	1.8842e-10(4.87)	1.9757e-10(4.99)

Table 2: L_1 errors of linear advection Eq. (42) with initial condition (43)

N	WENO-JS	WENO-NS	WENO-P	MWENO-P
10	1.3639e-01(—)	7.9335e-02(—)	7.8126e-02(—)	8.3177e-02(—)
20	1.2790e-02(3.41)	1.3137e-02(2.59)	1.3174e-02(2.56)	5.5774e-03(3.89)
40	1.0952e-03(3.54)	3.3350e-04(5.29)	3.6552e-04(5.17)	2.0964e-04(4.73)
80	8.7557e-05(3.64)	6.5660e-06(5.66)	7.6657e-06(5.57)	6.7007e-06(4.96)
160	7.4148e-06(3.56)	2.0946e-07(4.97)	1.8501e-07(5.37)	2.0988e-07(4.99)
320	4.0271e-07(4.20)	6.5526e-09(4.99)	6.2591e-09(4.88)	6.5526e-09(5.00)

Table 3: L_∞ errors of linear advection Eq. (42) with initial condition (44)

N	WENO-JS	WENO-NS	WENO-P	MWENO-P
10	6.6073e-02(—)	2.6674e-02(—)	2.6818e-02(—)	3.8523e-02(—)
20	4.9673e-03(3.73)	3.0373e-03(3.13)	3.9893e-03(2.74)	2.1165e-03(4.18)
40	3.7068e-04(3.74)	7.3314e-05(5.37)	7.4578e-05(5.74)	7.6161e-05(4.79)
80	1.7135e-05(4.43)	2.3943e-06(4.93)	1.9211e-06(5.27)	2.3652e-06(5.00)
160	7.3448e-07(4.54)	7.3574e-08(5.02)	6.6582e-08(4.85)	7.3534e-08(5.00)
320	2.5137e-08(4.86)	2.2922e-09(5.00)	2.2006e-09(4.91)	2.2927e-09(5.00)

Table 4: L_1 errors of linear advection Eq. (42) with initial condition (44)

4.1.2 Example 2:

For the partial differential equation (42), consider the initial condition

$$u(x, 0) = \sin(\pi x)^3. \quad (45)$$

For this initial condition, the first derivative and second derivatives vanish whereas the third derivative is non-zero. The L_1 and L_∞ errors along with the order of convergence for the MWENO-P scheme is shown in Table 5 and Table 6 respectively. The results shows the MWENO-P scheme achieves the desired order of accuracy where as WENO-NS and WENO-P fails to achieve.

N	WENO-JS	WENO-NS	WENO-P	MWENO-P
10	1.8058e-01(—)	1.5556e-01(—)	1.4980e-01(—)	1.6087e-01(—)
20	6.3274e-02(1.51)	3.1225e-02(2.31)	3.3257e-02(2.17)	2.6674e-02(2.59)
40	6.0354e-03(3.39)	6.6848e-03(2.22)	8.1907e-03(2.02)	3.0858e-03(3.11)
80	9.1031e-04(2.72)	9.1944e-04(2.86)	1.2103e-03(2.75)	3.0617e-04(3.33)
160	4.8182e-05(4.23)	1.0142e-04(3.18)	1.3156e-04(3.20)	1.3278e-06(7.84)
320	8.0849e-07(4.89)	9.8843e-06(3.35)	1.3798e-05(3.25)	3.8780e-08(5.09)
640	1.3257e-08(5.93)	9.9097e-07(3.31)	1.3735e-06(3.32)	1.1322e-09(5.09)
1280	2.3166e-10(5.83)	9.9188e-08(3.32)	1.4340e-07(3.26)	3.4832e-11(5.02)

Table 5: L_1 errors of linear advection Eq. (42) with initial condition (45)

N	WENO-JS	WENO-NS	WENO-P	MWENO-P
10	2.4666e-01(—)	2.2154e-01(—)	2.1397e-01(—)	2.2637e-01(—)
20	1.2969e-01(0.92)	6.0015e-02(1.88)	7.2114e-02(1.56)	4.7482e-02(2.25)
40	1.2970e-02(3.32)	1.6773e-02(1.83)	2.1148e-02(1.77)	1.1456e-02(2.05)
80	3.8067e-03(1.76)	3.7616e-03(2.15)	5.3389e-03(1.98)	2.2518e-03(2.34)
160	3.4089e-04(3.48)	8.0170e-04(2.23)	1.0032e-03(2.41)	4.2414e-06(9.05)
320	6.9825e-06(5.60)	1.4264e-04(2.49)	1.9960e-04(2.32)	9.6777e-08(5.45)
640	7.5668e-08(6.52)	2.4583e-05(2.53)	3.6812e-05(2.43)	1.7514e-09(5.78)
1280	7.2140e-10(6.71)	4.7171e-06(2.38)	6.7828e-06(2.44)	5.4793e-11(4.99)

Table 6: L_∞ errors of linear advection Eq. (42) with initial condition (45)

4.1.3 Example 3:

For linear advection equation (42), let the initial condition be

$$u(x, 0) = u_0(x) = \begin{cases} -\sin(\pi x) - \frac{1}{2}x^3 & \text{for } -1 \leq x < 0, \\ -\sin(\pi x) - \frac{1}{2}x^3 + 1 & \text{for } 0 \leq x < 1. \end{cases} \quad (46)$$

which is a piecewise sine function with jump discontinuity at $x = 0$. The solution is computed with the CFL number 0.5 with uniform concretization of the domain and the step size is $\Delta x = 0.01$ up to time $t = 8$. The approximate solution computed with MWENO-P along with WENO-JS, WENO-NS and WENO-P schemes is plotted in Figure 1 against the exact solution. It can be observed from the plot that the proposed scheme performs better than other schemes near the jump discontinuity.

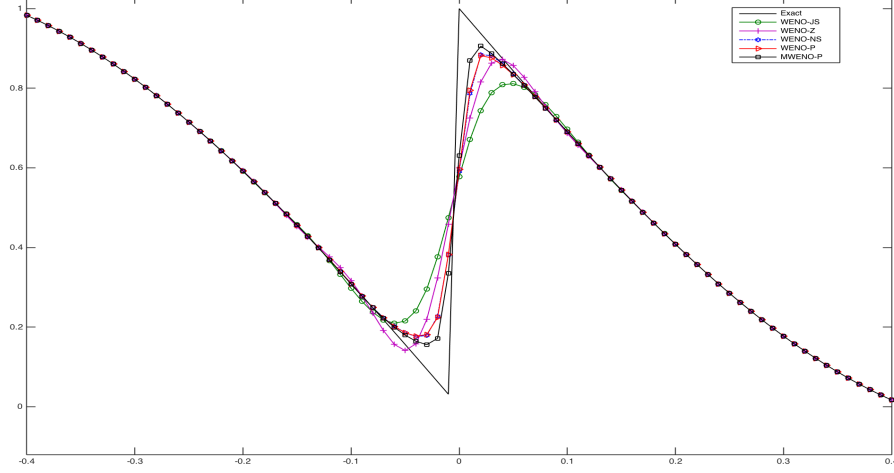


Figure 1: Numerical solution of linear advection Eq. (42) with the initial condition (46)

4.1.4 Example 4:

Consider the discontinuous profile

$$u(x, 0) = \begin{cases} 1 & \text{if } -0.5 \leq x < 0.5, \\ 0 & \text{otherwise.} \end{cases} \quad (47)$$

for the linear equation (42). The equation is solved with the CFL number 0.5 with the spatial step size $\Delta x = 0.01$. For time $t = 10$ the computed approximate solutions are plotted against exact solution in Figure 2. The proposed scheme MWENO-P has better approximation than WENO-JS, WENO-NS and WENO-P schemes especially near the areas of discontinuities.

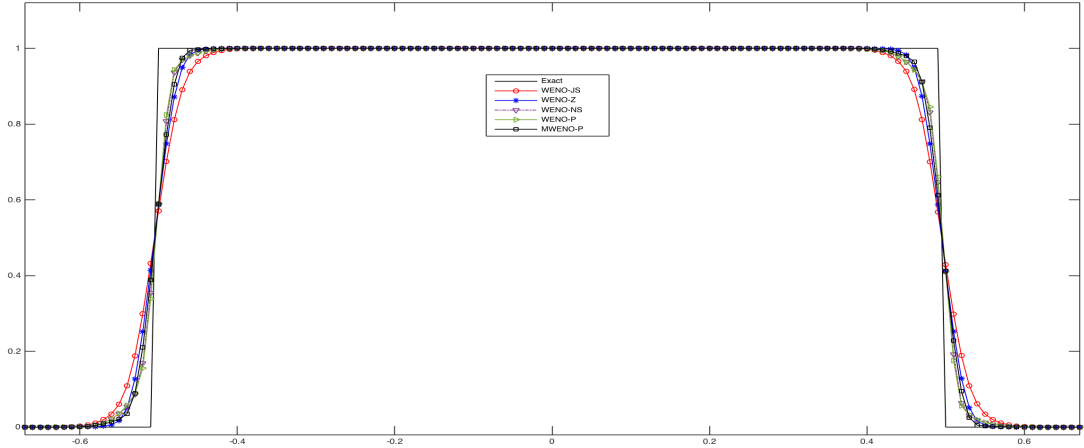


Figure 2: Numerical solution of linear advection Eq. (42) with the initial condition (47)

4.1.5 Example 5:

The WENO schemes are designed as a shock capturing schemes for solving the hyperbolic conservation laws, for this as a last example in this section considered the Burger's equation

$$\begin{aligned} u_t + \left(\frac{u^2}{2}\right)_x &= 0, \quad -1 \leq x \leq 1, \quad t \geq 0, \\ u(x, 0) &= u_0(x). \end{aligned} \quad (48)$$

subject to periodic boundary conditions. In Figure 3, the numerical result of the fifth-order WENO schemes for the initial conditions

$$u_0(x) = -\sin(\pi x). \quad (49)$$

at time $t = 1.5$ and

$$u_0(x) = \frac{1}{2} + \sin(\pi x). \quad (50)$$

at $t = 0.55$ are plotted respectively. The exact or reference solution is calculated with 2000 grid points with WENO-JS scheme and the approximate solutions are computed with 200 grid points in space. It is shown that the shocks are very well captured by all the schemes.

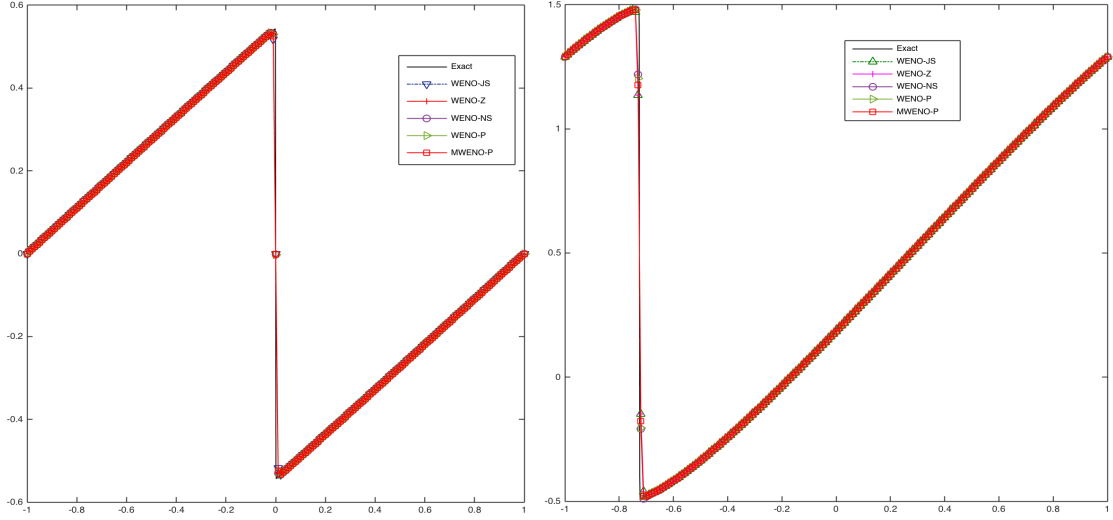


Figure 3: Approximate solution of (48) with initial condition (49) and (50)

4.2 Euler equations in one space dimension

The one-dimensional Euler equations are given by

$$\begin{pmatrix} \rho \\ \rho u \\ E \end{pmatrix}_t + \begin{pmatrix} \rho u \\ \rho u^2 + p \\ u(E + p) \end{pmatrix}_x = 0 \quad (51)$$

where ρ, u, E, p are the density, velocity, total energy and pressure respectively. The system (51) represents the conservation of mass, momentum and energy. The total energy for an ideal polytropic gas is defined as

$$E = \frac{p}{\gamma - 1} + \frac{1}{2}\rho u^2,$$

where γ is the ratio of specific heats and its value is taken as $\gamma = 1.4$.

The numerical flux $\hat{f}_{j+\frac{1}{2}}$ at $x_{j+\frac{1}{2}}$ is calculated based on the steps given in [22], which are reproduced here for completeness.

- Compute an average state $u_{j+\frac{1}{2}}$ using Roe's mean matrix.
- Compute the left eigenvectors, the right eigenvectors and the eigenvalues of the Jacobian $f'(u)$ at the average state $u_{j+\frac{1}{2}}$ and denote them by $L = L(u_{j+\frac{1}{2}})$, $R = R(u_{j+\frac{1}{2}})$, and $\Lambda = \Lambda(u_{j+\frac{1}{2}})$ respectively. Note that $L = R^{-1}$.
- Projecting the flux and the solution which are in the potential stencil of the WENO reconstruction for obtaining the flux $\hat{f}_{j+\frac{1}{2}}$ to the local characteristic fields by $s_j = R^{-1}u_j$, $q_j = R^{-1}f(u_j)$, j in a neighborhood of i .
- To obtain the corresponding component of the flux $\hat{q}_{j+\frac{1}{2}}^\pm$, Lax-Friedrich's flux splitting and the WENO reconstruction procedure is used for each component of the characteristic variables.
- Projecting back the characteristic variables to physical variables by $\hat{f}_{j+\frac{1}{2}}^\pm = R\hat{q}_{j+\frac{1}{2}}^\pm$.
- Finally, form the flux by taking $\hat{f}_{j+\frac{1}{2}} = \hat{f}_{j+\frac{1}{2}}^+ + \hat{f}_{j+\frac{1}{2}}^-$.

For time evaluation, we used third-order TVD Runge-Kutta scheme (40). Now consider the one dimensional Riemann problem for Euler system of equations (51) i.e., with the initial condition

$$U(x, 0) = \begin{cases} U_L & \text{if } x < x_0, \\ U_R & \text{if } x \geq x_0. \end{cases}$$

where $U_L = (\rho_l, u_l, p_l)$ and $U_R = (\rho_r, u_r, p_r)$. In the following, various test cases are taken for numerical study of MWENO-P scheme.

4.2.1 Sod's shock tube problem:

For this the initial condition is given by

$$U(x, 0) = \begin{cases} (1.0, 0.75, 1.0), & \text{if } 0 \leq x \leq 0.5, \\ (0.125, 0.0, 0.1), & \text{if } 0.5 \leq x \leq 1. \end{cases}$$

This is an example of modified version of Sod's problem defined in [26] and its solution contains a right shock wave, a right traveling contact wave and a left sonic rarefaction wave. Transmissive boundary conditions are taken for numerical evaluation. The solution is computed up to time $t = 0.2$ with 200 grid points in space with the CFL number 0.5. The density and pressure profile for various fifth-order WENO schemes are shown in Figure 4 and Figure 5 respectively against the reference solution which is calculated with 2000 grid points using WENO-JS scheme. It is observed that the proposed scheme MWENO-P performs better than other WENO schemes near the region of contact discontinuity.

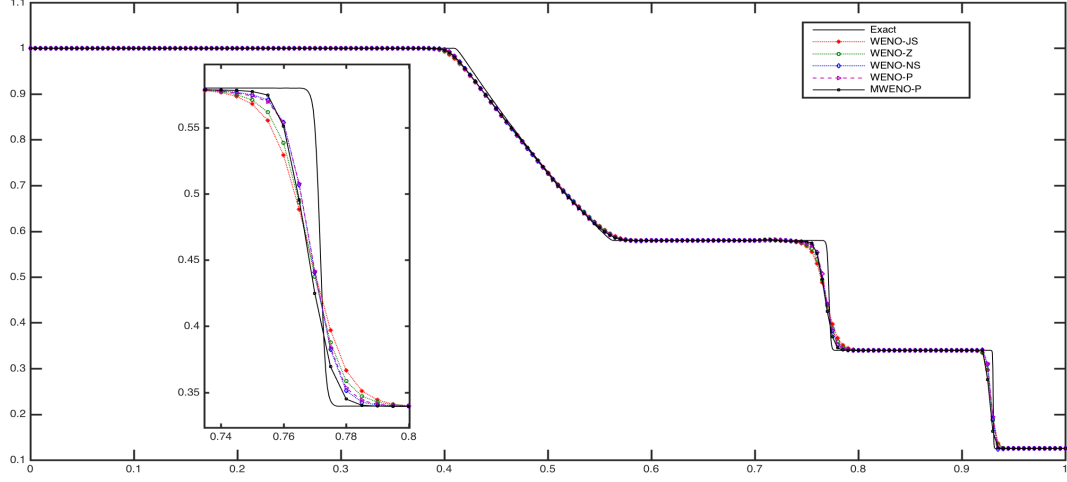


Figure 4: Density profile for Sod's problem and the zoomed region at the contact discontinuity

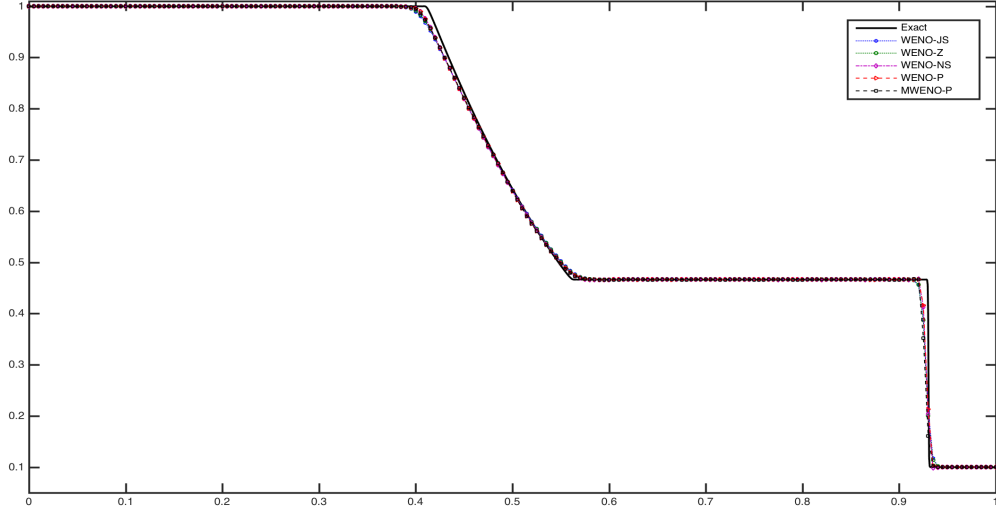


Figure 5: Pressure profile of Sod's shock tube problem

4.2.2 Shock tube problem with Lax initial condition:

For this the initial condition which is given by

$$U(x, 0) = \begin{cases} (0.445, 0.698, 3.528), & \text{if } -5 \leq x < 0, \\ (0.500, 0.000, 0.571), & \text{if } 0 \leq x \leq 5. \end{cases}$$

For this, the solution is computed up to time $t = 1.3$ with 200 grid points along space direction and the CFL number is set to be 0.5. The reference solution is calculated with 2000 grid points by using WENO-JS scheme. For assessing the performance of MWENO-P scheme, the density profile is plotted against the reference solution along with other schemes in Figure 6, it can be

seen that MWENO-P scheme performs better than other schemes near the discontinuities. The pressure profile is displayed in Figure 7.

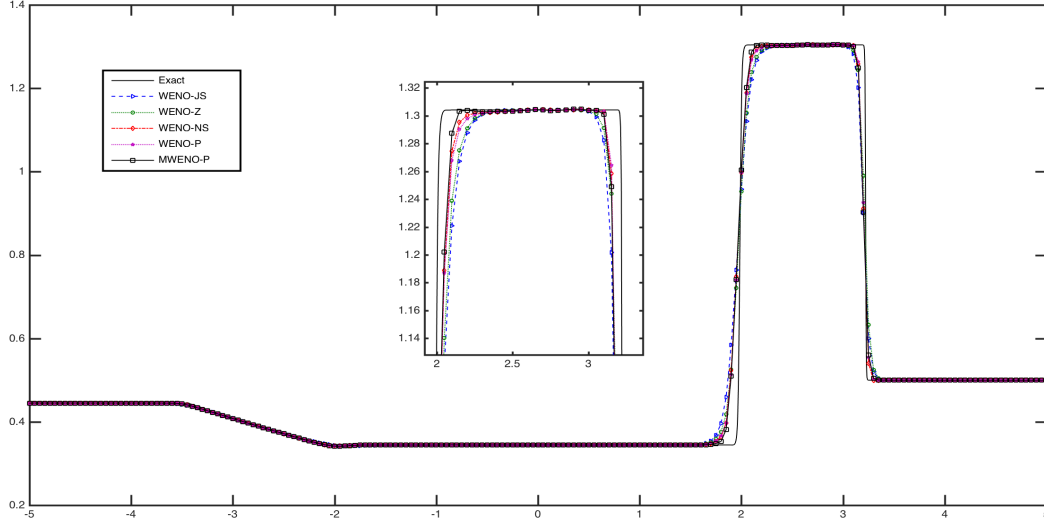


Figure 6: Density profile for Lax initial condition

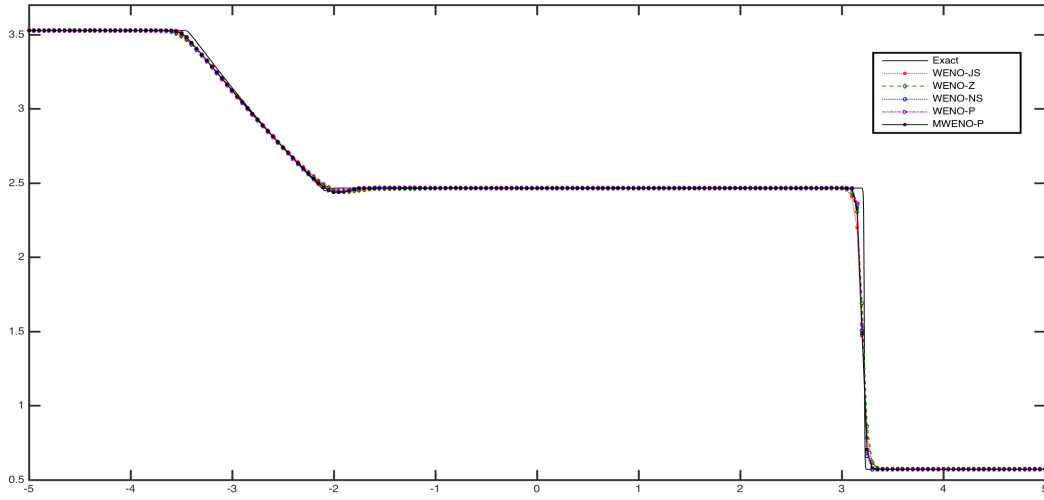


Figure 7: Pressure profile for Lax initial condition

4.2.3 1D shock entropy wave interaction problem:

The initial condition as given in [27] for shock entropy wave interaction problem is

$$U(x, 0) = \begin{cases} (3.857143, 2.629369, 10.33333), & \text{if } -5 \leq x < -4, \\ (1 + \epsilon \sin(kx), 0.000, 1.000), & \text{if } -4 \leq x \leq 5. \end{cases}$$

where ϵ and k are the amplitude and wavenumber of the entropy wave respectively, chosen $\epsilon = 0.2$ and $k = 5$. This problem has a right-moving supersonic (Mach 3) shock wave which interacts with sine waves in a density disturbance, that generates a flow field with both smooth structures and discontinuities. This flow induces wave trails behind a right-going shock with wave numbers higher than the initial density-variation wavenumber k . Since the exact solution is unknown, the reference solution with zero gradient boundary conditions is obtained by using the fifth-order WENO-JS scheme with 2000 grid points. The initial condition contains a jump discontinuity at $x = -4$ and especially, the initial density profile has oscillations on $[-4, 5]$. The solution is computed up to time $t = 1.8$ with 200 spatial grid points and the CFL number is set to be 0.5. The Figure 8 contains the graph of the solutions calculated at 200 grid points and its zoomed region near oscillations. It is observed that MWENO-P scheme performs better than WENO-JS and WENO-P at 200 grid points.

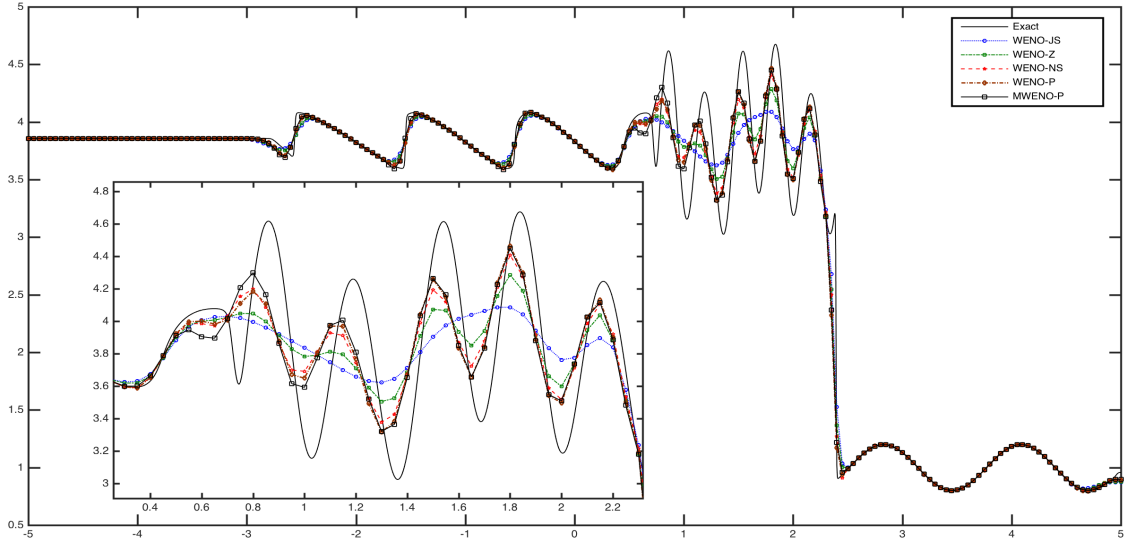


Figure 8: Shock entropy wave interaction test with 200 grid points

4.3 Two-Dimensional Euler equations

In this section, we apply the proposed scheme to two-dimensional problem in cartesian coordinates. The governing two-dimensional compressible Euler equations is given by

$$U_t + F(U)_x + G(U)_y = 0$$

where $U = (\rho, \rho u, \rho v, E)^T$, $F(U) = (\rho u, P + \rho u^2, \rho uv, u(E + P))^T$, $G(U) = (\rho v, \rho uv, P + \rho v^2, v(E + P))^T$. The total energy E and the pressure p is defined by

$$p = (\gamma - 1)(E - \frac{1}{2}\rho(u^2 + v^2))$$

where γ is the ratio of specific heats. Here ρ, u, v are density, x -wise-velocity component and y -wise-velocity component respectively.

4.3.1 2D problem of 2D gas dynamics

The 2D Riemann problem of gas dynamics is proposed in [21] and solved on the rectangular domain $[0, 1] \times [0, 1]$. The 2D Riemann problem is defined by initial constant states in each quadrant which is divided by lines $x = 0.8$ and $y = 0.8$ on the square as

$$(\rho, u, v, p) = \begin{cases} (1.5, 0, 0, 1.5) & \text{if } 0.8 \leq x \leq 1, 0.8 \leq y \leq 1, \\ (0.5323, 1.206, 0, 0.3) & \text{if } 0 \leq x < 0.8, 0.8 \leq y \leq 1, \\ (0.138, 1.206, 1.206, 0.029) & \text{if } 0 \leq x < 0.8, 0 \leq y < 0.8, \\ (0.5323, 0, 1.206, 0.3) & \text{if } 0.8 < x \leq 1, 0 \leq y < 0.8, \end{cases}$$

with Dirichlet boundary conditions. According to the initial conditions, four shocks come into being and produce a narrow jet. The numerical solution is calculated with 400×400 grid points up to $t = 0.8$ with the CFL number 0.5. An examination of these results reveals in figure 9 that, MWENO-P yields a better solution of the complex structure appearing when compares to WENO-JS and WENO-P schemes.

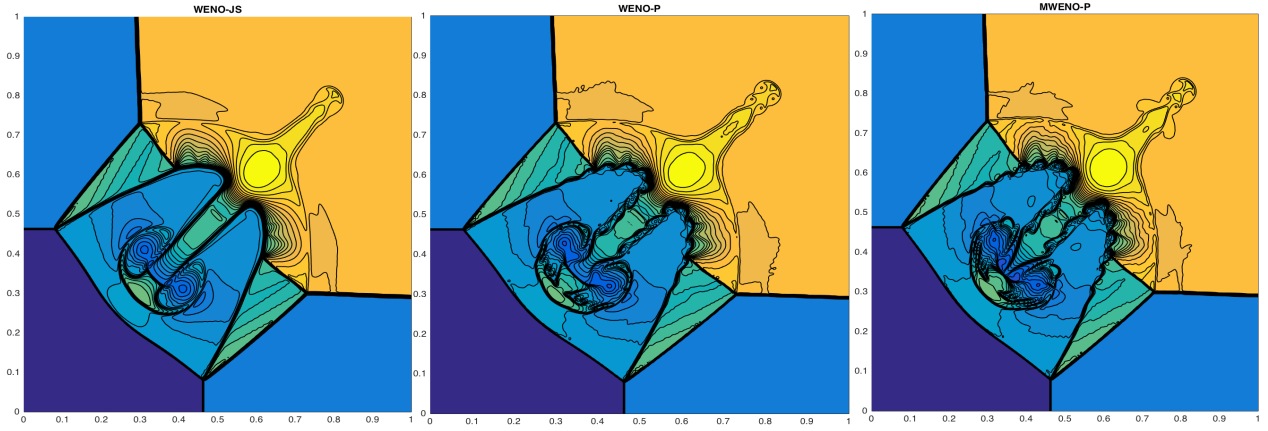


Figure 9: Density profile of 2D Riemann problem of 2D gas dynamics with the mesh $\Delta x = \Delta y = 1/400$

4.3.2 Two-Dimensional Rayleigh-Taylor instability

The Taylor instability happens on an interface between two fluids of different densities when an acceleration is directed from heavier fluid to lighter fluid. This problem has been simulated extensively in the literature [28]. The computational domain is $[0, 1/4] \times [0, 1]$ and the initial conditions are

$$(\rho, u, v, p) = \begin{cases} (2, 0, -0.025a \cos(8\pi x), 2y + 1) & \text{if } 0 \leq y < 0.5, \\ (1, 0, -0.025a \cos(8\pi x), y + \frac{3}{2}) & \text{if } 0.5 \leq y < 1. \end{cases}$$

with the sound speed $a = \sqrt{\gamma p / \rho}$ and the ratio of specific heats $\gamma = 5/3$. The gravitational effect is introduced by adding ρ and ρv to the right hand side of third equation and fourth equation,

respectively of the two-dimensional Euler equation. Reflective boundary conditions are imposed for the left and right boundaries and

$$(\rho, u, v, p) = \begin{cases} (2, 0, 0, 2.5) & \text{top boundary,} \\ (1, 0, 0, 1) & \text{bottom boundary.} \end{cases}$$

The final simulation time is $t = 1.95$. The density contour plotted in Fig. 10 shows that the WENO-P and MWENO-P obtains more complex structures than the other schemes.

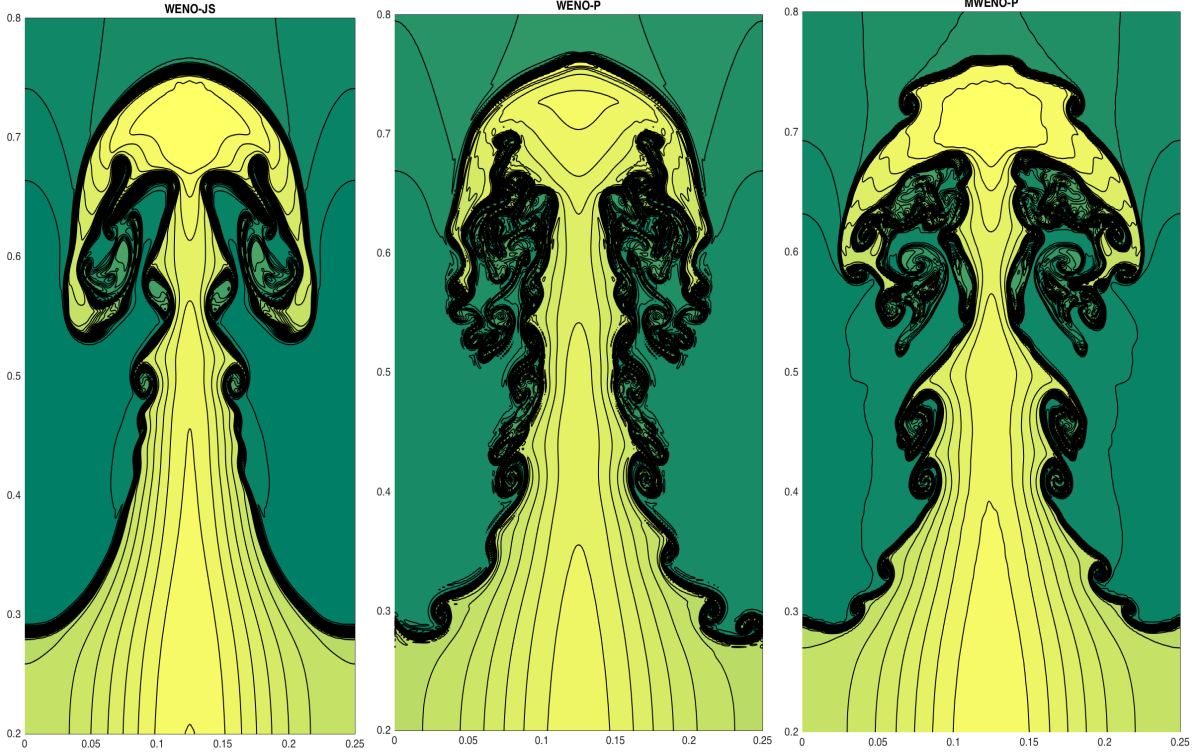


Figure 10: Density profiles of Rayleigh-Taylor instability problem at $t=1.95$ with the mesh $\Delta x = \Delta y = 1/500$

4.3.3 Double Mach reflection of a strong shock

The final test considered in this paper is the two-dimensional double mach reflection problem[27] where a vertical shock wave moves horizontally into a wedge that is inclined by some angle. The computational domain for this problem is chosen to be $[0, 4] \times [0, 1]$, and the reflecting wall lies at the bottom of the computational domain for $\frac{1}{6} \leq x \leq 4$. Initially a right-moving Mach 10 shock is positioned at $x = \frac{1}{6}, y = 0$, and makes a 60° angle with the x-axis. For the bottom boundary, the exact postshock condition is imposed for the part from $x = 0$ to $x = \frac{1}{6}$ and a reflective boundary condition is used for the rest. The top boundary of our computational domain uses the exact motion of the Mach 10 shock. Inflow and outflow boundary conditions are used for the left and right boundaries. The unshocked fluid has a density of 1.4 and a pressure of 1. The problem was run till $t = 0.2$ and the blow-up region around the double Mach stems. The ration of specific heats $\gamma = 1.4$ and we set CFL number as 0.5. The results in $[0, 3] \times [0, 1]$ are displayed for the WENO-JS, WENO-P and MWENO-P schemes in figures 11, 12 and 13 respectively. The figure 14 shows that the performance of the schemes WENO-JS, WENO-P and MWENO-P at the Mach stem of the density variable at the final time with several grid points. It can be clearly seen that MWENO-P resolves better the instabilities around the Mach stem.

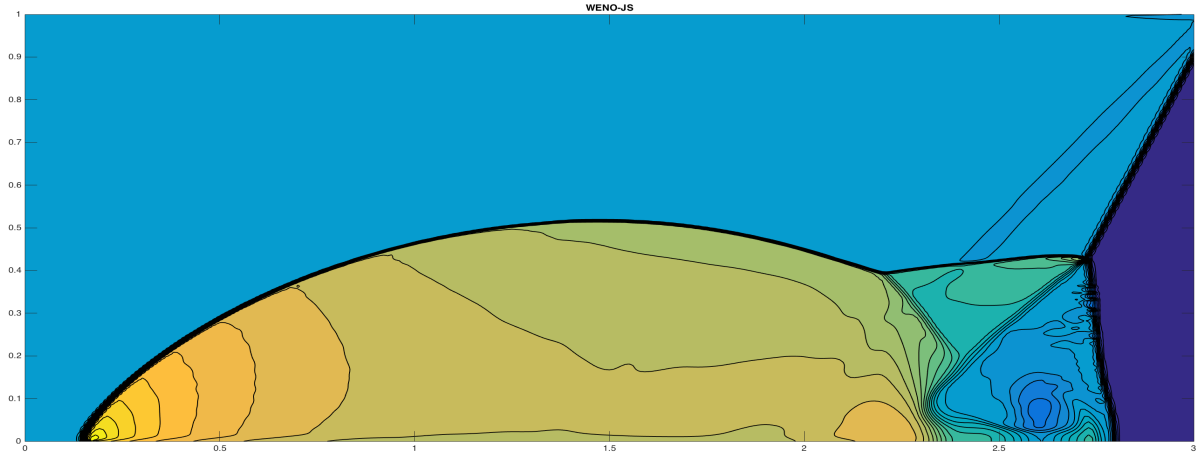


Figure 11: Density profiles of Double Mach reflection of a strong shock with WENO-JS scheme at $t=0.2$ with the mesh $\Delta x = \Delta y = 1/400$

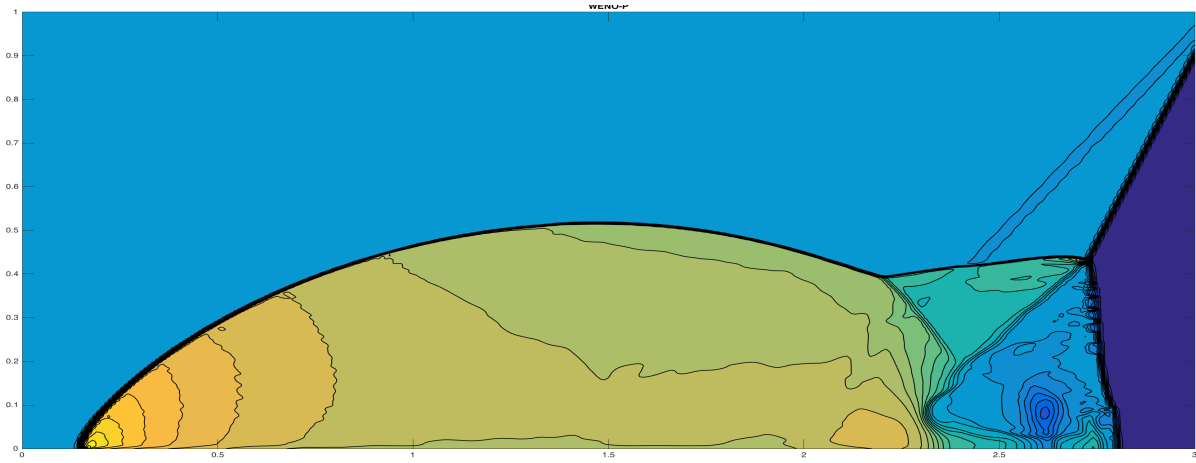


Figure 12: Density profiles of Double Mach reflection of a strong shock with WENO-P scheme at $t=0.2$ with the mesh $\Delta x = \Delta y = 1/400$

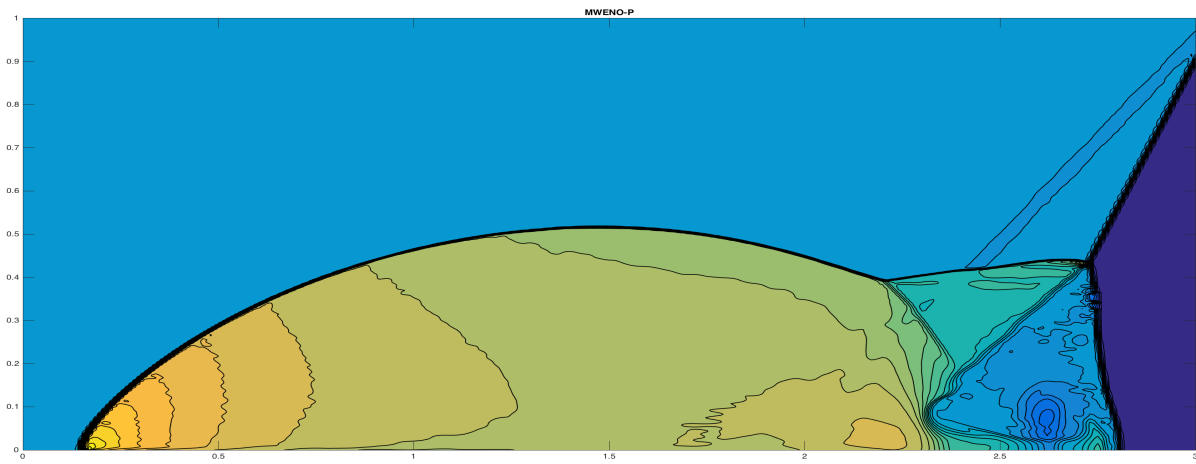


Figure 13: Density profiles of Double Mach reflection of a strong shock with MWENO-P scheme at $t=0.2$ with the mesh $\Delta x = \Delta y = 1/400$

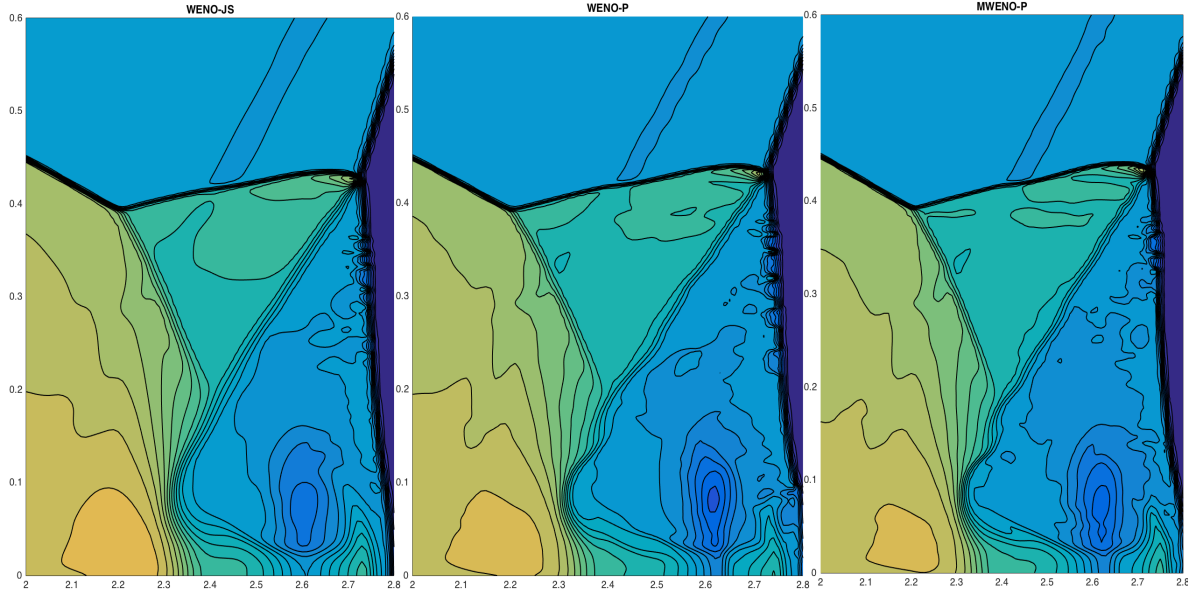


Figure 14: Density profiles of Double Mach reflection of a strong shock at Mach stem with WENO-JS, WENO-P and MWENO-P schemes at $t=0.2$ with the mesh $\Delta x = \Delta y = 1/400$

5 Conclusion

In this paper, a modified fifth-order WENO scheme to approximate the solution of nonlinear hyperbolic conservation laws named as MWENO-P was presented, by introducing a new global smoothness indicator based on undivided differences of second order derivatives of an interpolation polynomial over a stencil. The motivation to the study is that the WENO-NS and WENO-P schemes do not satisfy the sufficient condition if first-order derivatives vanish but the second derivative is non-zero. The proposed scheme satisfied the sufficient condition even if first and second derivatives vanish but the third derivative is non-zero. The approximate solutions to the one-dimensional scalar, system and two-dimensional system of hyperbolic conservation laws are simulated with the proposed scheme and compared it with other fifth-order WENO schemes. Numerical experiments show that the proposed scheme yields better approximation than other fifth-order schemes, especially to the numerical problems which contain discontinuities while keeping essentially non-oscillatory performance.

Acknowledgements: The authors are gratefully thank to the National Board for Higher Mathematics (NBHM) for the financial support by the Grant Reference No. 2/48(4)/2014/NBHM/R & D II//14356 through the Department of Atomic Energy (DAE), India.

References

- [1] F. Acker, R. B. de. Borges, and B. Costa. An improved WENO-Z scheme. J. Comput. Phys., 313:726-753, 2016.
- [2] D.S. Balsara, and C.W. Shu. Monotonicity preserving weighted essentially non-oscillatory schemes with increasingly high order of accuracy. J. Comput. Phys., 160:405-452, 2000 .

- [3] R. Borges, M. Carmona, B. Costa, and W.S. Don. An improved weighted essentially non-oscillatory scheme for hyperbolic conservation laws. *J. Comput. Phys.*, 227:3191-3211, 2008.
- [4] M. Castro, B. Costa, and W.S. Don. High order weighted essentially non-oscillatory WENO-Z schemes for hyperbolic conservation laws. *J. Comput. Phys.*, 230:766-792, 2011.
- [5] P. Fan, Y. Shen, B. Tian, and C. Yang. A new smoothness indicator for improving the weighted essentially non-oscillatory scheme. *J. Comput. Phys.*, 269:329-354, 2014.
- [6] P. Fan P. High order weighted essentially non oscillatory WENO-schemes for hyperbolic conservation laws. *J. Comput. Phys.*, 269:355-285, 2014.
- [7] G.A. Gerolymos, D. Senechal, and I. Vallet. Very high order WENO schemes. *J. Comput. Phys.*, 228:8481-8524, 2009.
- [8] S. Gottlieb, and C.W. Shu. Total variation diminishing Runge-Kutta schemes. *Math. of Comput.*, 67:73-85, 1998.
- [9] Y. Ha, C.H. Kim, Y.J. Lee, and J. Yoon. An improved weighted essentially non-oscillatory scheme with a new smoothness indicator. *J. Comput. Phys.*, 232:68-86, 2013.
- [10] A. Harten. High resolution schemes for hyperbolic conservation laws. *J. Comput. Phys.*, 49:357-393, 1983.
- [11] A. Harten. On a class of high resolution total-variation-stable finite-difference schemes. *SIAM J. Numer. Anal.*, 21:1, 1984.
- [12] A. Harten, S. Osher, B. Engquist, and S.R. Chakravarthy. Some results on uniformly high-order accurate essentially non-oscillatory schemes. *App. Numer. Math.*, 2: 347-377, 1986.
- [13] A. Harten, and S. Osher. Uniformly high-order accurate non oscillatory schemes, I. *SIAM J. Numer. Anal.*, 24: 279-309, 1987.
- [14] A. Harten, B. Engquist, S. Osher, and S.R. Chakravarthy. Uniformly high order accurate non-oscillatory schemes, III. *J. Comput. Phys.*, 131:3-47, 1997.
- [15] A.K. Henrick, T.D. Aslam, and J.M. Powers. Mapped weighted essentially non-oscillatory schemes: Achieving optimal order near critical points. *J. Comput. Phys.*, 207: 542-567, 2005.
- [16] F. Hu F, R. Wang, and X. Chen. A modified fifth-order WENOZ method for hyperbolic conservation laws. *J. Comput. and App. math.*, 303: 56-68, 2016.
- [17] G.S. Jiang, and C.W. Shu. Efficient implementation of Weighted ENO schemes. *J. Comput. Phys.*, 126:202-228, 1996.
- [18] C.H. Kim, Y. Ha, and J. Yoon. Modified Non-linear Weights for Fifth-Order Weighted Essentially Non-oscillatory Schemes. *J. Sci. Comput.*, 67:299-323, 2016.
- [19] X.D. Liu, S. Osher, and T. Chan. Weighted Essentially non-oscillatory schemes. *J. Comput. Phys.*, 115:200-212, 1994.
- [20] S. Osher, and S.R. Chakravarthy. High resolution schemes and the entropy condition. *SIAM J. Numer. Anal.*, 21:5, 1984.

- [21] C.W. Schulz-Rinne, J.P. Collins, and H.M. Glaz. Numerical solution of the riemann problem for two-dimensional gas dynamics. SIAM J. Sci. Compu., 14:1394-1414, 1993 .
- [22] C.W. Shu. Essentially non-oscillatory and weighted essentially non-oscillatory schemes for hyperbolic conservation laws. In Advanced numerical approximation of nonlinear hyperbolic equations. Lecture Notes in Mathematics, Berlin, Springer-Verlag , 1697: 325-432, 1993.
- [23] C.W. Shu. High order weighted essentially non oscillatory schemes for convection dominated problems. SIAM Review, 51:82-126, 2009.
- [24] C.W. Shu, and S. Osher. Efficient implementation of essentially non-oscillatory shock-capturing schemes. J. Comput. Phys., 77: 439-471, 1988.
- [25] C.W. Shu, and S. Osher. Efficient implementation of essentially non-oscillatory shock-capturing schemes II. J. Comput. Phys., 83:32-78, 1989.
- [26] G.A. Sod. A survey of several finite difference methods for systems of nonlinear hyperbolic conservation laws. J. Comput. Phys., 107:1-31, 1978.
- [27] P. Woodward, and P. Colella. The numerical simulation of two-dimensional fluid flow with strong shocks. J. Comput. Phys., 54:115-173, 1984.
- [28] Y.N. Young, H. Tufo, A. Dubey, and R. Rosner. On the miscible Rayleigh-Taylor instability: two and three dimensions. J. Fluid Mech. 447:377-408, 2001.